

# SafeLand: Safe Autonomous Landing in Unknown Environments with Bayesian Semantic Mapping

Markus Gross<sup>1,2,3,\*</sup>, Andreas Greiner<sup>1</sup>, Sai B. Matha<sup>1</sup>, Felix Soest<sup>1</sup>, Daniel Cremers<sup>2,3</sup>, Henri Meeß<sup>1</sup>  
<sup>1</sup>Fraunhofer IVI Autonomous Aerial Systems, <sup>2</sup>TU Munich Computer Vision Group, <sup>3</sup>Munich Center for Machine Learning

**Abstract**—Autonomous landing of uncrewed aerial vehicles (UAVs) in unknown, dynamic environments poses significant safety challenges, particularly near people and infrastructure, as UAVs transition to routine urban and rural operations. Existing methods often rely on prior maps, heavy sensors like LiDAR, static markers, or fail to handle non-cooperative dynamic obstacles like humans, limiting generalization and real-time performance. To address these challenges, we introduce SafeLand, a lean, vision-based system for safe autonomous landing (SAL) that requires no prior information and operates only with a camera and a lightweight height sensor. Our approach constructs an online semantic ground map via deep learning-based semantic segmentation, optimized for embedded deployment and trained on a consolidation of seven curated public aerial datasets (achieving 70.22% mIoU across 20 classes), which is further refined through Bayesian probabilistic filtering with temporal semantic decay to robustly identify metric-scale landing spots. A behavior tree then governs adaptive landing, iteratively validates the spot, and reacts in real time to dynamic obstacles by pausing, climbing, or rerouting to alternative spots, maximizing human safety. We extensively evaluate our method in 200 simulations and 60 end-to-end field tests across industrial, urban, and rural environments at altitudes up to 100m, demonstrating zero false negatives for human detection. Compared to the state of the art, SafeLand achieves sub-second response latency, substantially lower than previous methods, while maintaining a superior success rate of 95%. To facilitate further research in aerial robotics, we release SafeLand’s segmentation model as a plug-and-play ROS package, available at <https://github.com/markus-42/SafeLand>.

## I. INTRODUCTION

Autonomous landing of uncrewed aerial vehicles (UAVs) is a safety-critical task, especially in proximity to people and infrastructure [1], [2]. As UAVs move from isolated use cases toward dense deployments in logistics, inspection, and emergency response [3], regulatory frameworks such as the Specific Operations Risk Assessment (SORA) [2] impose stringent risk constraints. Landing systems must therefore ensure safety under diverse and only partially known conditions

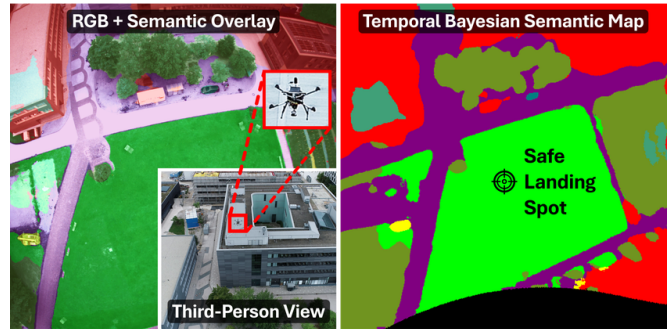


Figure 1: SafeLand predicts a semantic map, projects it to a metric ground plane, filters it probabilistically over time to select a landing spot, and uses a behavior tree for safe real-time landing in unknown dynamic environments.

while remaining lightweight and cost-efficient. Software and vision-based methods are central to this development, as they offer precise relative positioning from compact, low-power sensors, and are applicable across many platforms [2], [3].

To this end, most vision-centric methods for *safe autonomous landing (SAL)* are marker-based [3]: they achieve high accuracy and robustness on prepared landing pads by exploiting carefully designed markers and controlled infrastructure. However, these systems assume instrumented, static landing sites and thus do not generalize to generic outdoor operations, such as emergency landings in populated areas, or slowly changing environments, such as agricultural fields. Moreover, beyond marker-based methods, existing works employ markerless, hybrid and multi-sensor approaches, which exhibit systematic limitations [2]: many methods (i) assume prior maps, (ii) lack explicit metric reasoning due to the scale-ambiguous nature of camera-based projective geometry, (iii) depend on heavy and power-consuming depth sensors such as LiDAR or radar, (iv) treat humans as generic obstacles if at all, and (v) are rarely validated end-to-end in sophisticated field experiments.

Motivated by these gaps, we introduce *SafeLand* (Fig. 1), a lightweight, vision-based SAL system that builds an online semantic ground map from deep learning-based semantic segmentation and height-above-ground-level sensing, refines it via Bayesian temporal–probabilistic filtering, and uses a behavior tree to adapt landing decisions to non-cooperative dynamic obstacles, including people. Since generic vision foundation models underperform on aerial semantic segmentation [4], we train a network on curated public aerial datasets and release it. Our main contributions are summarized as follows:

- We present SafeLand, a lightweight, vision-based UAV landing solution that operates with a minimal sensor setup, requires no prior information about the landing site, and ensures safety for humans and infrastructure.
- We train a robust aerial semantic segmentation model from 7 curated datasets, achieving 70.22 mIoU, optimized for embedded deployment using the TensorRT engine.
- We evaluate SafeLand in simulations and 60 diverse field tests across industrial, urban, and rural environments at 25 m to 100 m altitudes, with deliberate interventions by non-cooperative dynamic obstacles, such as humans.
- SafeLand substantially outperforms baselines with sub-second response latency and a 95% landing success rate.
- Upon publication, we will release SafeLand’s segmentation model as a plug-and-play ROS package to facilitate further research in vision-based aerial robotics.

## II. RELATED WORK

Apart from methods that rely on depth sensors, such as LiDAR and radar [5]–[10], which often add significant weight and power consumption, vision-based methods have gained prominence as lightweight, cost-effective alternatives for SAL in unknown environments. These vision-centric approaches process camera imagery to detect suitable landing sites, and are often categorized as traditional image processing for feature extraction, such as edge detection or texture analysis [11]–[13], supervised zone-classification based on visual cues [14]–[18], or more advanced deep learning-driven semantic segmentation to delineate terrain types [19]–[22]. A prevalent limitation across many is the dependence on priors, such as pre-existing maps of potential landing areas [23]–[26] or structured environments with instrumented landing pads [5]–[7], which restricts their applicability to truly dynamic or unprepared scenarios where environmental changes or lack of infrastructure demand greater flexibility [2]. Furthermore, to address the

inherent scale ambiguity in camera-based projective geometry, several methods integrate metric compensation strategies, including assumptions of flat ground for homography-based transformations [27], [28], depth cameras [28], or fusion with complementary data sources like inertial measurements and altitude sensors to recover absolute scales [11]–[13], [18]–[20], [29]–[31], enabling precise sizing of landing spots relative to UAV dimensions.

Importantly, safety considerations, particularly for people as non-cooperative dynamic obstacles, are underexplored in the literature and, when addressed, are typically handled only in a subset of works through techniques like population density estimation from aerial views [26], [32] or real-time visual tracking to monitor and predict human movements [25], [27], [29]–[31]. Notably, comprehensive validation remains a gap [2]: to the best of our knowledge, only Safe2Ditch [27] conducts sophisticated end-to-end field tests under real-world conditions, demonstrating practical functionality with human interference, whereas the majority evaluate individual components, such as standalone perception modules, or confine assessments entirely to simulations [2], [5]–[26], [29]–[32], limiting insights to isolated challenges, such as lighting conditions, without considering holistic system viability.

In summary, SafeLand follows this line of vision-based SAL but differs in three key aspects. It trains a dedicated aerial segmentation model from complementary datasets to handle diverse unknown environments, restores metric scale using only a lightweight height above ground level (AGL) sensor instead of heavy depth hardware or prior maps, and explicitly targets human safety with conservative Bayesian filtering of person detections, validated in 200 simulations and 60 field tests across industrial, urban, and rural sites up to 100 m AGL.

## III. METHODOLOGY

### A. Method Overview

SafeLand (see Fig. 2) uses only a nadir-pointing camera and an AGL sensor. It applies deep learning-based semantic segmentation on temporal camera frames, projects the resulting semantic probabilities onto a discrete, metrically scaled ground plane to obtain a semantic ground map, and iteratively filters this map via Bayesian inference and semantic decay for robust perception. We then extract safe landing spot candidates, and a behavior tree-based landing procedure navigates the UAV toward the selected spot while re-selecting a new spot if the current one becomes invalid. This pipeline

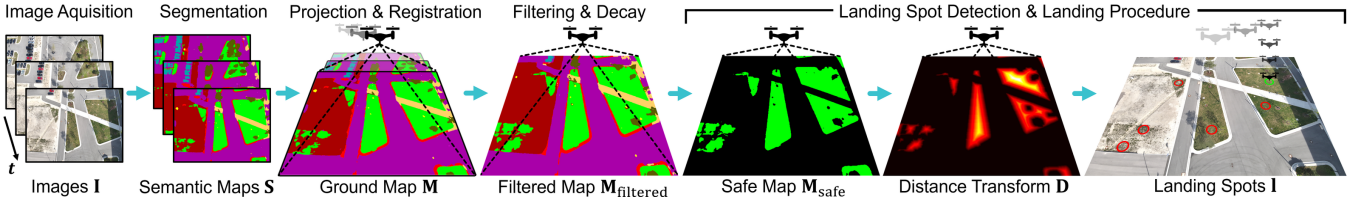


Figure 2: Chronological processing steps of our method SafeLand. An overview is provided in Sec. III-A.

continuously evaluates the environment, reacts in real time to non-cooperative obstacles, and operates without prior map information or heavy sensors, supporting generic deployment.

### B. Image Acquisition and Semantic Segmentation

A nadir-pointing RGB camera captures real-time imagery for semantic segmentation. Robust perception in previously unseen and diverse terrain requires diverse training data, yet existing aerial datasets are individually too narrow, and current vision foundation models for semantic segmentation underperform in the aerial domain [4]. We therefore consolidate seven open-source datasets [33]–[39] that provide aerial imagery with semantic segmentation ground truth and curate their labels into 20 unified classes.

We train a SegFormer MiT-B3 model [40] with 47.3 million parameters and obtain 70.22% mIoU, detailed in Tab. I. We select SegFormer for its balance between accuracy and efficiency, which enables deployment on resource-constrained onboard hardware. This model is further optimized for embedded deployment using the TensorRT inference engine [41] with FP16 precision calibration, increasing standalone throughput to 12FPS.

Formally, let  $\mathcal{C}$  be the set of semantic classes summarized in Tab. I. The camera image  $\mathbf{I} \in \mathbb{R}^{M \times N \times 3}$  is segmented as

$$\mathbf{S} = \Phi_s(\mathbf{I}), \quad (1)$$

where  $\Phi_s$  denotes the segmentation model,  $\mathbf{S} \in \mathbb{R}^{M \times N \times C}$  is the predicted map,  $M \times N$  represents the image resolution, and  $C = |\mathcal{C}|$  is the number of semantic classes.

Overall, semantic segmentation relies only on a lightweight and cost-efficient camera, removes the need for prior map information, facilitates generalization to diverse environments, and improves safety by explicitly modeling humans.

### C. Projection and Registration

These steps follow the method described in [42], and assume a flat ground and AGL measurements. In summary, the undistorted semantic map is projected onto a ground

plane using the UAV’s pose and height, in addition to camera intrinsics and extrinsics, yielding a discrete semantic ground map  $\mathbf{M} \in \mathbb{R}^{X \times Y \times C}$  with fixed size and metric scale.

Formally, a homogeneous pixel coordinate  $\mathbf{s} \in \mathbb{P}^2$  on the predicted semantic map  $\mathbf{S}$  and its corresponding homogeneous 3D point  $\tilde{\mathbf{m}} \in \mathbb{P}^3$  on the semantic ground map  $\mathbf{M}$  are related by

$$\mathbf{s} = [K \mid \mathbf{0}] \cdot \mathbf{T}_{\text{cam} \leftarrow \text{world}} \cdot \tilde{\mathbf{m}}, \quad (2)$$

where  $\mathbf{0} \in \mathbb{R}^3$  is the null vector,  $\mathbf{K} \in \mathbb{R}^{3 \times 3}$  are camera intrinsics, and  $\mathbf{T}_{\text{cam} \leftarrow \text{world}} \in \text{SE}(3)$  denotes a rigid transformation from planar world coordinates to camera coordinates [42].

Subsequent registration aligns earlier maps with the current one, by transforming a Cartesian point  $\mathbf{m}_{t-1} \in \mathbb{R}^3$  via

$$\mathbf{M}_t(\mathbf{m}_{t-1}) = \mathbf{M}_{t-1}(\mathbf{H}_{t \leftarrow (t-1)} \cdot \mathbf{m}_{t-1}), \quad (3)$$

where  $\mathbf{M}_t$  and  $\mathbf{M}_{t-1}$  denote the ground maps at times  $t$  and  $(t-1)$ , respectively.  $\mathbf{H}_{t \leftarrow (t-1)} \in \mathbb{R}^{3 \times 3}$  is a homography that warps points from the previous map’s coordinate system to the current one, which is computed from the camera extrinsics at times  $t$  and  $(t-1)$ . In practice, four or more corresponding points are sufficient to estimate this homography whenever the extrinsics change. For more details, see [42].

### D. Bayesian Filtering and Semantic Decay

The segmentation model’s predictions remain subject to residual errors and dataset-induced biases. We therefore iteratively refine the semantic ground map  $\mathbf{M}$  over time, enhancing robustness and safety of subsequent landing spot detection.

Formally, we apply Bayesian inference and treat the model’s softmax outputs as unnormalized conditional class probabilities that serve as proxies for likelihood terms in the Bayesian update. This filtering process updates the belief about the state of each pixel in the semantic ground map based on new observations from the segmentation model  $\Phi_s$ . Let  $P(c \mid \mathbf{M}_t)$  be the posterior probability of class  $c$  given the segmentation

map  $\mathbf{M}_t$  at time  $t$ . The filtering process is expressed as

$$P(c | \mathbf{M}_t) = \frac{P(\mathbf{M}_t | c) \cdot P(c | \mathbf{M}_{t-1})}{P(\mathbf{M}_t)}, \quad (4)$$

where  $P(\mathbf{M}_t | c)$  represents the likelihood of observing the semantic ground map  $\mathbf{M}_t$  given class  $c$ ,  $P(c | \mathbf{M}_{t-1})$  is the prior probability of class  $c$  at time  $t - 1$ , and  $P(\mathbf{M}_t)$  is the evidence (marginal likelihood). While the evidence is often omitted when only relative posterior scores are needed, we compute it explicitly by normalizing the posterior to ensure numerical stability. We initialize with a uniform prior.

Subsequently, semantic decay incrementally updates the posterior beliefs over time, incorporating new posteriors by applying a decay factor to downweight the contribution of past observations. Let  $\alpha$  be the decay factor, and  $\mathbf{M}_t$  be the refined semantic ground map at time  $t$ . This update is formulated as

$$\mathbf{M}_t(\mathbf{m}, c) = \alpha \cdot \mathbf{M}_{t-1}(\mathbf{m}, c) + (1 - \alpha) \cdot P(c | \mathbf{M}_t(\mathbf{m}, c)), \quad (5)$$

where  $\mathbf{M}_t(\mathbf{m}, c)$  and  $\mathbf{M}_{t-1}(\mathbf{m}, c)$  are the probabilities of class  $c$  at position  $\mathbf{m}$  in the refined map at time  $t$  and  $(t - 1)$ , respectively, and  $\alpha$  is the decay factor, which is empirically set to  $\alpha = 0.1$ . Eqn. 5 also implies that, if no updates are received for  $\alpha^{-1}$  iterations, the semantic estimate decays to 0, ensuring that stale evidence is forgotten and the map remains up to date with recent observations.

Furthermore, to ensure safety in our proposed method, we treat human detections conservatively by setting the class probability of any predicted person to  $P(\mathbf{M}_t | c) = 1$ , where  $c \hat{=} person$ . Moreover, semantic decay for persons is only applied if a different semantic class is predicted at the same position, ensuring that their probability does not decay to 0 when no updates are received.

Formally, the filtered map  $\mathbf{M}_{\text{filtered}} \in \mathbb{R}^{X \times Y \times 1}$  is determined by selecting the class with the highest probability at each location  $\mathbf{m}$  as the definitive class for that location:

$$\mathbf{M}_{\text{filtered}}(\mathbf{m}) = \arg \max_c \mathbf{M}_t(\mathbf{m}, c). \quad (6)$$

By applying Bayesian filtering with semantic decay, we mitigate segmentation errors, ensure robust performance in unknown environments, and enhance human safety.

### E. Landing Spot Detection

A safe landing spot is identified in three steps (see Fig. 2). First, we define and rank semantic classes suitable for safe landing (e.g., grass, dirt, gravel), denoted as  $\mathcal{C}_{\text{safe}}$ , and only

Table I: Intersection over union (IoU) and mean IoU (mIoU) in [%] for semantic segmentation (Sec. III-B). To ensure scientific rigor, we retain the train/val/test splits of the original datasets [33]–[39]. Thus, some classes appear only in the training split and are absent from val/test, so their performance cannot be quantified and is marked as n/a. However, for these classes, we (1) qualitatively assess them and (2) confirm their high practical performance by successfully landing on them in real-world field tests (Sec. IV-B). The lower Bicycle score is consistent with its sparse occurrence in the data.

	IoU	mIoU
Road	92.85	70.22
Dirt	n/a	
Gravel	n/a	
Rock	n/a	
Grass	80.18	
Vegetation	96.41	
Tree	81.52	
Obstacle	39.14	
Animal	81.74	
Person	70.09	
Bicycle	1.88	
Vehicle	69.18	
Water	83.30	
Boat	n/a	
Wall	83.49	
Roof	81.05	
Sky	97.40	
Drone	35.49	
Train-Track	50.61	
Background	-	

consider these classes in the safe semantic ground map  $\mathbf{M}_{\text{safe}}$ :

$$\mathbf{M}_{\text{safe}} = \{\mathbf{M}_{\text{filtered}}(c) | c \in \mathcal{C}_{\text{safe}}\}. \quad (7)$$

We then apply a distance transform [43] to each segment individually. Illustrated in Fig. 2, each pixel represents the least distance to its segment border, expressed as  $\mathbf{D} \in \mathbb{R}^{X \times Y \times 1}$ :

$$\mathbf{D} = \text{distance\_transform}(\mathbf{M}_{\text{safe}}). \quad (8)$$

Since the distances are measured on a metric scale (see Sec. III-C), we define an adjustable safety radius  $r_{\text{safe}}$  that accounts for the physical UAV dimensions. The segment with the largest distance value that exceeds this radius is chosen as the landing segment. The coordinates of this maximum value define the center of the landing spot, denoted by  $\mathbf{l} \in \mathbb{Z}^2$ :

$$\mathbf{l} = \arg \max_{\mathbf{D}(x,y) \geq r_{\text{safe}}} \mathbf{D}(x, y). \quad (9)$$

All segments that satisfy these constraints are stored as a history of safe landing spots. The ranking of semantic classes and the choice of the point of maximum distance within a safe segment are conservative design parameters that can be replaced by more adaptive criteria if required. By utilizing a metric distance transform, we naturally account for UAV size constraints ( $r_{\text{safe}} = 3$  m in experiments), enabling safe landings without prior map information, such as designed markers.

### F. Landing Procedure

Once a safe landing spot  $\mathbf{l}$  (Eqn. 9) has been identified, a behavior tree [44] governs the landing procedure illustrated in Fig. 3. The behavior tree executes three main sequences:

**Landing Spot Available Sequence.** It searches for valid landing spots at or above an adjustable *search altitude* of 15 m

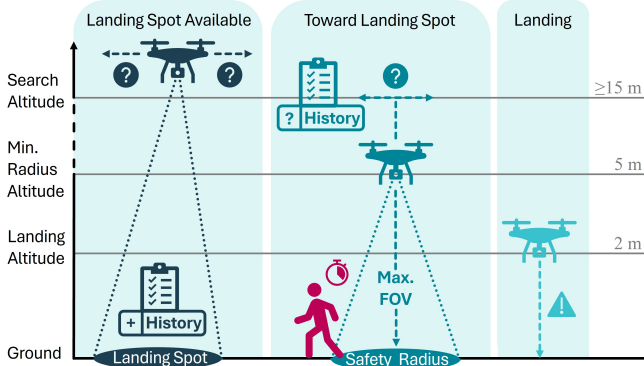


Figure 3: Landing procedure. A behavior tree (Sec. III-F) executes three distinct sequences that ensure safe, real-time landing in unknown and dynamic environments.

(see Fig. 3), effectively executing all steps from segmentation to landing spot detection (Sec. III-B to III-E). If a landing spot is found but not yet required, or if several spots are found, their locations are stored in a history of safe landing spots. If no spot is detected, the UAV continues along its current heading as a simple search strategy, adaptable to mission requirements.

**Toward Landing Spot Sequence.** The UAV first flies level to a waypoint above the selected landing spot, and then descends toward the *landing altitude* (Fig. 3). During descent, the system repeatedly validates the landing spot as described in the previous sequence and climbs back to the search altitude if it becomes invalid, either to find a new landing spot or to use one from the history. Once the *minimum radius altitude* (5 m) is reached, the system only checks for dynamic objects because the safety radius then covers the full camera image (Fig. 3). If dynamic objects are detected, the UAV pauses for 5 seconds and returns to the previous sequence at search altitude if they persist. If the area clears within 5 seconds, the UAV resumes its descent and proceeds to the next sequence.

**Landing Sequence.** This sequence is executed when the *landing altitude* (2 m) is reached, thus the UAV commits to land without making further decisions. This strict requirement reflects the increased risks associated with ground effects and the segmentation model’s reduced reliability at lower altitudes (< 2 m) due to limited low-altitude imagery in the training data. Furthermore, at this stage, the landing spot has remained valid to this altitude, increasing confidence in its safety.

These behavior tree sequences enable real-time responses in a local frame without relying on pre-mapped areas, such as controlled infrastructure, supporting generic deployment.



Figure 4: Hardware configuration. **Left:** Quadcopter PM Q-685 [48] custom frame, equipped with NVIDIA Jetson AGX Orin [49], GNSS module SimpleRTK2B Pro [50], and flight controller Pixhawk Cube Orange with its IMUs [51]. **Right:** Nadir-pointing RGB camera FLIR Blackfly S-PGE-31S4C-C [52] and the height AGL sensor Lightware SF11/C [53].

## IV. EXPERIMENTAL RESULTS

### A. Simulation Experiments

**Setup:** We adopt a software-in-the-loop (SIL) setup with the OCTAS v1.0 simulation framework [45], and use ROS2 Humble [46] and PX4 v1.15.4 [47] to mirror the hardware stack used in field tests. We define “grass” as the safe semantic class  $C_{\text{safe}}$  for landing, which can be adapted to other classes based on operational requirements. As the segmentation model (Sec. III-B) is trained on real-world imagery, we rely on simulated semantic ground truth. We run 200 trials at an altitude of 50 m with up to 10 dynamic obstacles, such as humans, to evaluate response and rerouting behavior.

**Results:** The first column of Fig. 6 shows that our method filters the segmentation over time, selects a valid landing spot within the safe classes, and lands successfully. When non-cooperative obstacles enter the safety radius, the system either waits until they leave or reroutes to an alternative landing spot. No landings failed, and no incorrect reroutes occurred.

### B. Field Experiments

**Setup:** Our method is implemented in ROS2 Humble [46], and we employ the hardware configuration shown in Fig. 4. The Jetson is connected to the camera via Ethernet, and to the Pixhawk via a UART uXRCE-DDS Bridge [54]. The Pixhawk communicates with the GNSS module via UART, and with AGL sensor via I2C. The UAV’s pose is the fused global state provided by the Pixhawk EKF estimator, which fuses IMU, GNSS, and with the AGL sensor. Field demonstrations comprise a total of 60 flights, with 20 flights in each of industrial, urban, and rural environments, covering altitudes

Table II: Baseline comparison as discussed in Sec. IV-C. Ambiguous references are marked as –.

Reference	No Prior	Metric	No Lid./Rad.	People	Field
[5]–[7]	✗	✓	✗	✗	✗
[23]	✗	✗	✓	✗	✗
[24]	✗	✓	–	✗	✗
[19], [20]	✗	✓	✓	✗	✗
[10], [21], [22]	✓	–	✓	✗	✗
[14]	✓	✗	✓	✗	✗
[15]–[17]	✓	✗	✓	✗	✗
[8], [9]	✓	✓	✗	✗	✗
[18]	✓	✓	–	✗	✗
[11]–[13], [28]	✓	✓	✓	✗	✗
[25], [26]	✗	✓	✓	✓	✗
[32]	✓	✗	✓	✓	✗
[29]–[31]	✓	✓	✓	✓	✗
Safe2Ditch [27]	✗	✓	✓	✓	✓
SafeLand (ours)	✓	✓	✓	✓	✓

of 25 m, 50 m, and 100 m. We define “grass” and “gravel” as safe semantic classes  $C_{\text{safe}}$  for landing, adaptable to mission requirements. Up to 3 humans actively intervene in the landing procedure.

**Results:** Of the 60 landings (see Fig. 6), 57 completed successfully (95%), and 3 were safely aborted due to transient communication issues between the Pixhawk and the Jetson, independent of our proposed method. When individuals entered the landing zone, the system either paused and resumed the landing or rerouted to an alternative landing spot if the original one remained invalid. In two cases, the segmentation model falsely predicted humans in the landing zone, temporarily blocking landings until later observations reclassified the area as safe, and the landings were completed. Importantly, no false negatives occurred: every human in the landing zone was detected, which underscores the robustness and safety of our system. These experiments demonstrate real-time operation and reliable detection of landing spots at all evaluated altitudes, supported by the robust performance of the semantic segmentation model. Bayesian filtering and semantic decay reduce segmentation errors and yield a stable yet responsive world representation, which our behavior tree-based landing procedure successfully processes while accounting for human safety. Using the Jetson, we achieve an end-to-end processing speed of 1.3 Hz (30 W), 2.0 Hz (50 W), and 3.2 Hz (MAXN).

### C. Baseline Comparison

Existing work on safe autonomous landing (see Sec. II) and recent comprehensive review studies [2], [3] reveal a multitude of requirements for generic vision-based landing systems: A method should (1) operate without prior information about the

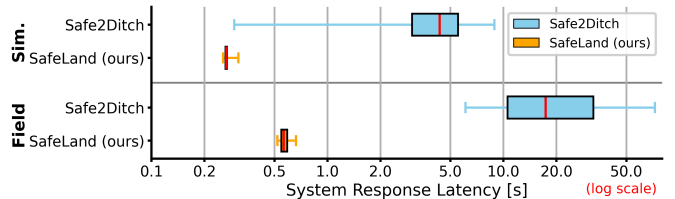


Figure 5: System response latencies (see Sec. IV-C) on dynamic obstacles for Safe2Ditch [27] and SafeLand (ours). We substantially outperform Safe2Ditch by providing sub-second response as a critical capability for unknown environments.

landing zone to handle unknown and dynamic environments, (2) use metric information to size landing spots relative to UAV dimensions, (3) support different UAV sizes using lightweight sensors such as cameras instead of heavy, power-demanding LiDAR or radar, (4) prioritize human safety, and (5) be validated in sophisticated end-to-end field tests under real-world conditions. Table II summarizes these requirements and shows that our proposed method is the first to meet all criteria. To the best of our knowledge, Safe2Ditch [27] is the only method to present a complete system and report sophisticated field experiments. Thus, we use Safe2Ditch as a baseline, although it benefits from preselected landing sites as priors.

In simulation, failure rates are zero for our method and effectively zero for Safe2Ditch. In field tests, Safe2Ditch reports 1 failure in 16 trials due to misclassification, while our method reports 3 failures in 60 trials, caused by transient Pixhawk-Jetson communication issues independent of our method. Moreover, response latency measures the time from when a non-cooperative obstacle enters the landing zone until an intervention is triggered. Safe2Ditch [27] reports this only as plots, so we digitize them. For both methods, we identically average simulations and field latencies. Fig. 5 shows that our method achieves substantially lower response latency, as we perform hardware-optimized semantic segmentation, whereas Safe2Ditch requires time-consuming multiple target tracking.

## V. CONCLUSION

We demonstrate safe autonomous landing using a lightweight camera-based method without prior maps or heavy sensors, achieving 95% success and low response latency in simulation and field tests while ensuring human safety. Future work will target limitations such as the planar ground assumption, either by explicitly modeling the local slope, or by treating it as noise and uncertainty during Bayesian filtering.

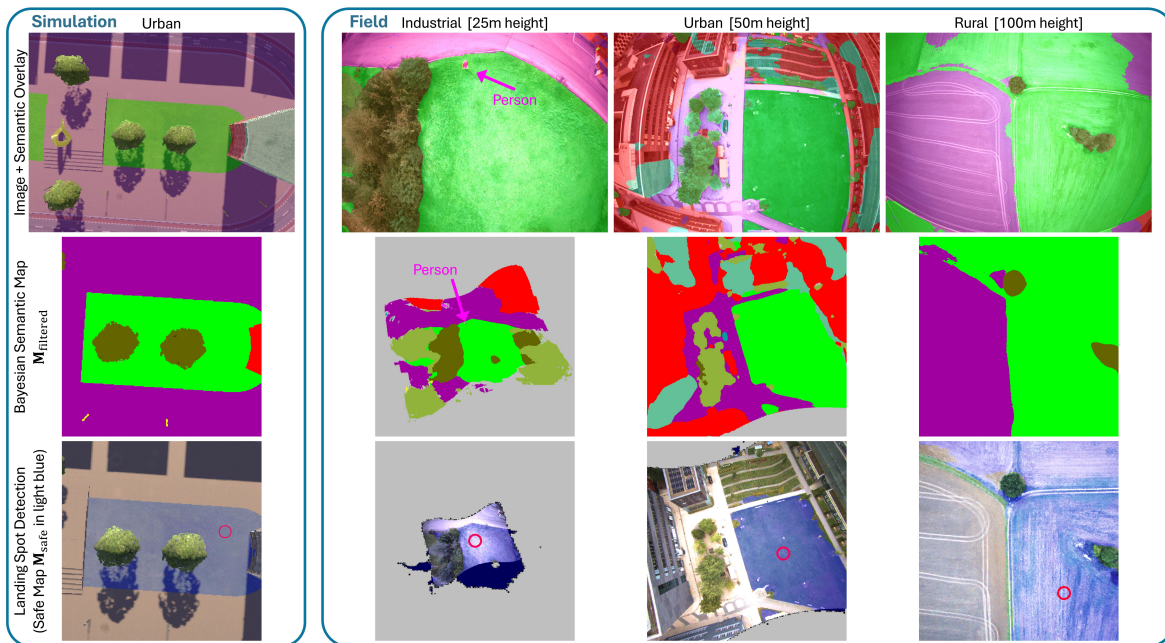


Figure 6: Experimental results (Sec. IV) in 200 simulations and 60 industrial, urban, and rural field trials (25–100 m AGL) show that SafeLand reliably identifies metric-scale landing sites and responds to non-cooperative humans in real time, achieving 95% end-to-end landing success, zero false negatives for human detection, and sub-second response latency. Note that the map has a fixed, metric-scale size, resulting in a smaller map at lower heights, as the camera field of view covers less area.

## REFERENCES

- [1] H. Tovanche-Picon, J. González-Trejo, Á. Flores-Abad, M. Á. García-Terán, and D. Mercado-Ravell, “Real-time safe validation of autonomous landing in populated areas: from virtual environments to Robot-In-The-Loop,” *Virtual Reality*, vol. 28, no. 1, Mar. 2024.
- [2] M. Farajjalal, H. Eslamiat, V. Avineni, E. Hettel, and C. Lindsay, “Safety systems for emergency landing of civilian unmanned aerial vehicles (uavs)—a comprehensive review,” *Drones*, vol. 9, no. 2, 2025.
- [3] S. O. Semerikov, P. P. Nechypurenko, T. A. Vakaliuk, I. S. Mintii, and A. O. Kolhatin, “Vision-based autonomous UAV landing: A comprehensive review of technologies, techniques, and applications,” *Journal of Intelligent and Robotic Systems*, vol. 111, no. 4, Oct. 2025.
- [4] L. P. Osco, Q. Wu, E. L. de Lemos, W. N. Gonçalves, A. P. M. Ramos, J. Li, and J. Marcato, “The segment anything model (sam) for remote sensing applications: From zero to one shot,” *International Journal of Applied Earth Observation and Geoinformation*, vol. 124, 2023.
- [5] B. Xia, I. Mantegh, and W. Xie, “Integrated Emergency Self-Landing Method for Autonomous UAS in Urban Aerial Mobility,” in *2021 21st International Conference on Control, Automation and Systems (ICCAS)*, 2021, pp. 275–282.
- [6] B. Xia, T. He, I. Mantegh, and W. Xie, “Ai-based de-confliction and emergency landing algorithm for uas,” September 2022.
- [7] F. S. Neves, L. M. Branco, M. I. Pereira, R. M. Claro, and A. M. Pinto, “A multimodal learning-based approach for autonomous landing of uav,” in *2024 20th IEEE/ASME International Conference on Mechatronic and Embedded Systems and Applications (MESA)*, 2024, pp. 1–8.
- [8] T. Matsumoto and C. Premachandra, “Depth Sensor Application in Ground Unevenness Estimation for UAV Emergency Landing,” in *2023 IEEE Sensors Applications Symposium (SAS)*, 2023, pp. 1–6.
- [9] G. Loureiro, A. Dias, A. Martins, and J. Almeida, “Emergency landing spot detection algorithm for unmanned aerial vehicles,” *Remote Sensing*, vol. 13, no. 10, 2021.
- [10] J. Chen, W. Du, J. Lin, U. M. Borhan, Y. Lin, B. Du, X. Li, and J. Li, “Emergency uav landing on unknown field using depth-enhanced graph structure,” *IEEE Transactions on Automation Science and Engineering*, pp. 1–12, 2024.
- [11] V. Turan, E. Avşar, D. Asadi, and E. A. Aydın, “Image processing based autonomous landing zone detection for a multi-rotor drone in emergency situations,” *Turkish Journal of Engineering*, vol. 5, no. 4, 2021.
- [12] P. Fraczek, A. Mora, and T. Kryjak, “Embedded Vision System for Automated Drone Landing Site Detection,” in *Computer Vision and Graphics*, L. J. Chmielewski, R. Kozera, A. Orłowski, K. Wojciechowski, A. M. Bruckstein, and N. Petkov, Eds. Cham: Springer International Publishing, 2018, pp. 397–409.
- [13] T. Hinzmann, T. Stastny, C. Cadena, R. Siegwart, and I. Gilitschenski, “Free LSD: Prior-Free Visual Landing Site Detection for Autonomous Planes,” *IEEE Robotics and Automation Letters*, vol. 3, no. 3, 2018.
- [14] K. Mukadam, A. Sinh, and R. Karani, “Detection of landing areas for unmanned aerial vehicles,” in *2016 International Conference on Computing Communication Control and automation (ICCUBEA)*, 2016.
- [15] M. A. Kaljahi, P. Shivakumara, M. Y. I. Idris, M. H. Anisi, T. Lu, M. Blumenstein, and N. M. Noor, “An automatic zone detection system for safe landing of uavs,” *Expert Systems with Applications*, vol. 122, pp. 319–333, 2019.
- [16] J. Guerin, K. Delmas, and J. Guiochet, “Certifying emergency landing for safe urban uav,” in *2021 51st Annual IEEE/IFIP International Conference on Dependable Systems and Networks Workshops (DSN-W)*, 2021, pp. 55–62.
- [17] O. Bektash, J. J. Naundrup, and A. la Cour-Harbo, “Analyzing visual imagery for emergency drone landing on unknown environments,” *Inter-*

- national Journal of Micro Air Vehicles*, vol. 14, p. 17568293221106492, 2022.
- [18] S. Aziz, R. Faheem, M. Bashir, A. Khalid, and A. Yasin, "Unmanned aerial vehicle emergency landing site identification system using machine vision," *journal of image and graphics*, vol. 4, pp. 36–41, June 2015.
- [19] C. Patrino, M. Nitti, A. Petitti, E. Stella, and T. D'Orazio, "A Vision-Based Approach for Unmanned Aerial Vehicle Landing," *Journal of Intelligent & Robotic Systems*, vol. 95, August 2019.
- [20] N. Bodunkov and N. Kim, "Autonomous Landing-Site Selection for a Small Drone," *Russian Engineering Research*, vol. 41, pp. 72–75, March 2021.
- [21] O. Bektash, J. N. Pedersen, A. Ramirez Gomez, and A. I. Cour-Harbo, "Automated emergency landing system for drones: Safeeye project," in *2020 International Conference on Unmanned Aircraft Systems (ICUAS)*, 2020, pp. 1056–1064.
- [22] A. R. Gomez and A. la Cour-Harbo, "Emergency Landing Decision Method for Unmanned Aircraft," in *2021 International Conference on Unmanned Aircraft Systems (ICUAS)*, 2021, pp. 1233–1239.
- [23] M.-F. R. Lee, A. Nugroho, T.-T. Le, Bahrudin, and S. N. Bastida, "Landing Area Recognition using Deep Learning for Unmanned Aerial Vehicles," in *2020 International Conference on Advanced Robotics and Intelligent Systems (ARIS)*, 2020, pp. 1–6.
- [24] F. Neves, L. Branco, M. Pereira, R. Claro, and A. Pinto, "A multimodal learning-based approach for autonomous landing of uav," 2024.
- [25] D. Pieczyński, B. Ptak, M. Kraft, M. Piechocki, and P. Aszkowski, "A fast, lightweight deep learning vision pipeline for autonomous uav landing support with added robustness," *Engineering Applications of Artificial Intelligence*, vol. 131, p. 107864, 2024.
- [26] E. Carney, L. Castano, and H. Xu, *Determination of Safe Landing Zones for an Autonomous UAS using Elevation and Population Density Data*. American Institute of Aeronautics and Astronautics SciTech 2019, January 2019.
- [27] P. C. Lusk, P. C. Glaab, L. J. Glaab, and R. W. Beard, "Safe2ditch: Emergency landing for small unmanned aircraft systems," *Journal of Aerospace Information Systems*, vol. 16, no. 8, pp. 327–339, 2019.
- [28] P. Łuczak and G. Granosik, "Autonomous UAV landing and collision avoidance system for unknown terrain utilizing depth camera with actively actuated gimbal," *Sensors*, vol. 25, no. 19, p. 6165, 2025.
- [29] J. Gonzalez-Trejo, D. Mercado-Ravell, I. Becerra, and R. Murrieta-Cid, "On the visual-based safe landing of uavs in populated areas: A crucial aspect for urban deployment," *IEEE Robotics and Automation Letters*, vol. 6, pp. 7902–7909, 10 2021.
- [30] H. Tovanche-Picon, J. Gonzalez-Trejo, A. Flores-Abad, and D. Mercado-Ravell, "Visual-based safe landing for uavs in populated areas: Real-time validation in virtual environments," 2022.
- [31] A. Merei, H. Mcheick, A. Ghaddar, and G. Beltrame, "Esls: A vision-based emergency safe landing system for uavs," *Procedia Computer Science*, vol. 272, pp. 277–285, 2025, 16th International Conference on Emerging Ubiquitous Systems and Pervasive Networks / 15th International Conference on Current and Future Trends of Information and Communication Technologies in Healthcare.
- [32] J. A. Gonzalez-Trejo and D. A. Mercado-Ravell, "Lightweight Density Map Architecture for UAVs Safe Landing in Crowded Areas," *Journal of Intelligent & Robotic Systems*, vol. 102, no. 1, p. 7, 4 2021.
- [33] I. Nigam, C. Huang, and D. Ramanan, "Ensemble knowledge transfer for semantic segmentation," in *2018 IEEE Winter Conference on Applications of Computer Vision (WACV)*, 2018, pp. 1499–1508.
- [34] M. Rahnemoonfar, T. Chowdhury, A. Sarkar, D. Varshney, M. Yari, and R. R. Murphy, "Floodnet: A high resolution aerial imagery dataset for post flood scene understanding," *IEEE Access*, vol. 9, pp. 89 644–89 654, 2021.
- [35] Institute of Computer Graphics and Vision, TU Graz, "Semantic drone dataset," accessed 09.12.2023.
- [36] S. Speth, A. Gonçalves, B. Rigault, S. Suzuki, M. Bouazizi, Y. Matsuo, and H. Prendinger, "Deep learning with rgb and thermal images onboard a drone for monitoring operations," *Journal of Field Robotics*, vol. 39, no. 6, pp. 840–868, 2022.
- [37] Y. Lyu, G. Vosselman, G.-S. Xia, A. Yilmaz, and M. Y. Yang, "Uavid: A semantic segmentation dataset for UAV imagery," *ISPRS Journal of Photogrammetry and Remote Sensing*, vol. 165, pp. 108 – 119, 2020.
- [38] Y. Chen, Y. Wang, P. Lu, Y. Chen, and G. Wang, "Large-scale structure from motion with semantic constraints of aerial images," in *Chinese Conference on Pattern Recognition and Computer Vision (PRCV)*. Springer, 2018, pp. 347–359.
- [39] W. Cai, K. Jin, J. Hou, C. Guo, L. Wu, and W. Yang, "Vdd: Varied drone dataset for semantic segmentation," 2024.
- [40] E. Xie, W. Wang, Z. Yu, A. Anandkumar, J. M. Alvarez, and P. Luo, "Segformer: Simple and efficient design for semantic segmentation with transformers," in *Neural Information Processing Systems*, 2021.
- [41] NVIDIA Corporation, "NVIDIA TensorRT," <https://developer.nvidia.com/tensorrt>, 2026, accessed: 2026-02-15.
- [42] P. Hausmann, H. Meeß, and G. Elger, "Image segmentation based emergency landing for autonomous and automated unmanned aerial vehicles," in *33rd congress of the international council of the aeronautical sciences*, September 2022.
- [43] R. Fabbri, L. D. F. Costa, J. C. Torelli, and O. M. Bruno, "2d euclidean distance transform algorithms: A comparative survey," *ACM Comput. Surv.*, vol. 40, no. 1, feb 2008.
- [44] M. Colledanchise and P. Ögren, "Behavior trees in robotics and ai," Jul. 2018.
- [45] A. Sielemann, S. Wolf, M. Roschani, J. Ziehn, and J. Beyerer, "Synset boulevard: A synthetic image dataset for vmmr\*," in *2024 IEEE International Conference on Robotics and Automation (ICRA)*, 2024.
- [46] S. Macenski, T. Foote, B. Gerkey, C. Lalancette, and W. Woodall, "Robot operating system 2: Design, architecture, and uses in the wild," *Science Robotics*, vol. 7, no. 66, p. eabm6074, 2022.
- [47] L. Meier, D. Honegger, and M. Pollefeys, "Px4: A node-based multithreaded open source robotics framework for deeply embedded platforms," in *2015 IEEE International Conference on Robotics and Automation (ICRA)*, 2015, pp. 6235–6240.
- [48] P. Modellbau, "Quadcopter Q-685," <https://www.premium-modellbau.de/pm-q-685-klappbarer-carbon-quadcopter-rahmen-rtf-komplettsset-frsky>, 2024, accessed: 2026-02-15.
- [49] NVIDIA, "Jetson AGX Orin Developer Kit," <https://www.nvidia.com/en-us/autonomous-machines/embedded-systems/jetson-orin>, accessed: 2026-02-15.
- [50] ArduSimple, "simpleRTK2B Pro," 2024, accessed: 2024-09-10.
- [51] Pixhawk, "The Cube Orange," <https://ardupilot.org/copter/docs/common-thecubeorange-overview.html>, accessed: 2026-02-15.
- [52] FLIR, "Blackfly S PGE-31S4C-C," <https://www.flir.com/products/blackfly-s-gige/?model=BFS-PGE-31S4C-C&vertical=machine+vision&segment=iis>, accessed: 2026-02-15.
- [53] Lightware, "SF11/C," <https://lightwarelidar.com/shop/sf11-c-100-m/>, accessed: 2026-02-15.
- [54] "PX4 v1.15 uXRCE-DDS Bridge," [https://docs.px4.io/v1.15/en/middleware/uxrce\\_dds](https://docs.px4.io/v1.15/en/middleware/uxrce_dds), accessed 2026-02-15.